WILEY-VCH

DOI: 10.1002/ (adfm.201602873)
Article type: Full Paper

Atomic Insights into the Enhanced Surface Stability in High Voltage Cathode Materials by Ultrathin Coating

Xin Fang,[†] Feng Lin[#§], Dennis Nordlund,[‖] Matthew Mecklenburg,[⊥] Mingyuan Ge,[†] Jiepeng Rong,[†] Anyi Zhang,[†] Chenfei Shen,[†] Yihang Liu,[‡] Yu Cao,[‡] Marca M. Doeff,[#] and Chongwu Zhou[†‡,]*

Dr. X. Fang, Dr. M. Ge, Dr. J. Rong, A. Zhang, C. Shen, Prof. C. Zhou
Mork Family Department of Chemical Engineering and Materials Science, University of Southern California, Los Angeles, California 90089, United States
E-mail: chongwuz@usc.edu((insert e-mail address(es) of corresponding author(s)))
Dr. F. Lin, Dr. M. M. Doeff
Energy Storage & Distributed Resources Division, Lawrence Berkeley National Laboratory, Berkeley, California 94720, USA
Dr. D. Nordlund
Stanford Synchrotron Radiation Lightsource, SLAC National Accelerator Laboratory, Menlo Park, California 94025, USA
Dr. M. Mecklenburg
Center for Electron Microscopy and Microanalysis, University of Southern California, Los Angeles, California 90089, USA
Y. Liu, Y. Cao, Prof. C. Zhou
Ming Hsieh Department of Electrical Engineering, University of Southern California, Los Angeles, California 90089, United States
Prof. F. Lin
Department of Chemistry, Virginia Tech, Blacksburg, VA 24061, USA
Keywords: lithium ion batteries, high voltage cathode, $LiNi_{0.5}Mn_{1.5}O_4$, surface modification, Mn^{2+} evolution

Abstract

Surface properties of electrode materials play a critical role in the function of batteries. Therefore, surface modifications, such as coatings, have been widely used to improve the battery performance. Understanding how these coatings function to improve battery performance is crucial for both scientific research and application. In this study we correlate the

electrochemical performance of coated and uncoated $LiNi_{0.5}Mn_{1.5}O_4$ electrodes with ensemble-averaged soft X-ray absorption spectroscopy and spatially resolved electron energy loss spectroscopy to illustrate the mechanism of how ultrathin layer Al_2O_3 coatings improve the cycle life of $LiNi_{0.5}Mn_{1.5}O_4$. Mn^{2+} evolution on the surface is clearly observed in the uncoated sample, which results from the reaction between the electrolytic solution and the surfaces of $LiNi_{0.5}Mn_{1.5}O_4$ particles, and also possibly atomic structure reconstructions and oxygen loss from the surface region in $LiNi_{0.5}Mn_{1.5}O_4$. The coating has been found to effectively suppress the Mn^{2+} evolution, and improves the battery performance by decelerating the impedance buildup from the surface passivation. This study demonstrates the importance of combining ensemble-averaged techniques (e.g., XAS) with localized techniques (e.g., STEM-EELS), as the latter may yield unrepresentative information due to the limited number of studied particles, and sheds light on the design of future coating processes and materials.

1. Introduction

Lithium ion batteries have been widely recognized as the most important energy storage devices and power sources for portable electronics. Nowadays, with the development of new-generation electronic devices and more importantly, electric vehicles, performance requirements have become more stringent, especially in terms of energy density and cycle life. In this respect, further improvement and precise understanding of batteries are highly desired and urgently needed. Since the total energy of

a battery is dependent both upon cell voltage and capacity, increasing the output voltage is an important method to enhance the energy of batteries. According to Goodenough, the spinel $LiNi_{0.5}Mn_{1.5}O_4$ is electroactive at the upper voltage limit of compatibility with organic carbonate electrolytic solutions. Since the potential profile is nearly flat in spite of the two-electron change in Ni redox state, which is highly desirable for power management, $LiNi_{0.5}Mn_{1.5}O_4$ is considered one of the most promising high voltage cathode materials for lithium ion batteries.

Surface properties are critical to the functioning of battery materials in many aspects, as solid electrolyte interfaces (SEI) and cathode electrolyte interfaces (CEI) influence cyclability and rate capability. Surface coatings have been recognized as an effective method to control and optimize the surface properties of both cathode and anode materials in batteries and are widely utilized in both academic research and industry applications. However, the quality of surface coatings depends critically on the properties of the coating and active materials, as well as the processes used. The effect of many types of surface coatings on $LiNi_{0.5}Mn_{1.5}O_4$, used to ameliorate the side reactions during the high voltage operation, including materials such as Au, Ag, Bi_2O_3, BiOF, ZnO, ZrO_2, ZrP_2O_7, AlF_3, conductive carbon, polyimide, graphene-oxide, and coating processes such as wet chemistry, sputtering, evaporation, and atomic layer deposition (ALD), have led to varying results. In addition, much of the previous work only demonstrated improved cycling and/or rate performance with limited in-depth exploration of the mechanism of the

improvement; thus the knowledge to guide future work is unclear. The few existing mechanistic studies mainly focused on one charge-discharge cycle whereas the cumulative effect during long-term cycling has rarely been considered. It is important to investigate the function of coating materials and coating processes in order to better understand the mechanism of improved battery performance by surface modification and provide insights for the further advancement of high performance batteries.

Here, we report our investigations on the surface properties of $LiNi_{0.5}Mn_{1.5}O_4$ and reveal how ultrathin layers of Al_2O_3 coated by ALD improved the cycling stability. We have correlated the battery performance shown in the electrochemical measurements with results from ensemble-averaged XAS and spatially resolved STEM-EELS. The analysis provides insights into the evolution of Mn^{2+} on the surface of $LiNi_{0.5}Mn_{1.5}O_4$ and the function of metal oxide coating in suppressing this undesired surface reaction, which leads to impedance buildup. The discovery in our work provides guidelines for prospective studies on the possibility of improving battery performance through surface property tuning and ultrathin coatings down to the atomic scale. More importantly, since many materials have similar surface phenomena such as chemical evolution and surface reconstruction, the research methodology and mechanism illustrated in this work provides insightful information that can be beneficial to studies on other electrode materials.

2. Results and discussion

2.1 Pre-cycling characterization

$LiNi_{0.5}Mn_{1.5}O_4$ particles can be synthesized *via* various methods, with co-precipitation and solid-state reactions the most relevant choices for industrial applications. Here we synthesized $LiNi_{0.5}Mn_{1.5}O_4$ particles using a solid-state reaction as reported in our previous work. **Figure 1a** shows the scanning electron microscope image of the as-synthesized $LiNi_{0.5}Mn_{1.5}O_4$ particles. The particles had polyhedral shapes with sizes ranging from around 1 μm to 2 μm. The X-ray diffraction (XRD) pattern of the as-synthesized $LiNi_{0.5}Mn_{1.5}O_4$ particles is presented in the inset of **Figure 1a**. All the peaks can be indexed according to the reported pattern for cubic structured spinel $LiNi_{0.5}Mn_{1.5}O_4$.

As illustrated in the schematic diagram, Al_2O_3 was coated on pre-fabricated electrodes through 10 cycles of ALD using the same process as reported in our previous work, with a growth rate of about 0.12 nm per cycle. ALD is known as the most favorable thin film technology for continuous and pin-hole free thin film deposition with precise thickness control. The self-limiting surface reaction leads to conformal coverage even on high aspect ratio structures. The particles here reflect the particles in the $LiNi_{0.5}Mn_{1.5}O_4$ electrode. The scheme shows that all the surface area that would be exposed to electrolyte is covered by an Al_2O_3 film, while the conductive pathway inside the electrode is not blocked by the Al_2O_3 film. **Figure 1b** shows the energy dispersive X-ray (EDX)

mapping of the electrode surface where the evidence for the existence of Al is obviously seen, demonstrating successful coating of the samples. To confirm that the ALD process does not alter the oxidation states of transition metals on the surface, Mn and Ni oxidation states were probed by soft XAS for both coated and uncoated samples before cycling (**Figure 1c and 1d**). The total electron yield (TEY) mode, which has a depth sensitivity of 5-10 nm in this configuration, was used to obtain the data. The spectra are essentially identical, indicating no change to the Ni and Mn oxidation states after coating. The data are consistent with oxidation states of Mn and Ni that are primarily +4 and +2, respectively, as expected.

2.2 Electrochemical characterization of coated and uncoated $LiNi_{0.5}Mn_{1.5}O_4$ electrodes

To explore the mechanism of the enhanced cycling stability of $LiNi_{0.5}Mn_{1.5}O_4$, we looked into the changes of transition metal oxidation states after cycling, since the oxidation and reduction of transition metals are fundamental processes during cell operation. Before taking the XAS measurements, both the coated and uncoated electrodes were cycled at C/5 between 3.5-5.0 V for 35 cycles in CR2032 size coin cells with lithium metal as the counter electrodes. Representative charge-discharge curves are plotted in **Figure 2a and 2c**. The coated and uncoated electrodes were prepared from the same batch of material and underwent the same charging profile, so the difference in cycling stability can be attributed to the coating process. In both cases, a small amount of capacity near 4V

suggests that some Mn^{3+} was present in the as-made material, although most of the redox activity took place at about 4.7V, as is typical for $LiNi_{0.5}Mn_{1.5}O_4$. Here it's clearly seen that after only 35 cycles at C/5, the uncoated samples show a capacity loss while the coated ones showed much better capacity retention and coulombic efficiency after the first cycle (~98.8% *vs*. 98.2%, **Figure S1**). The difference is more obvious when the cells are cycled at C/2; see the representative profiles in **Figure 2b and 2d**. With the increased rate (C/2 compared with C/5), the differences in polarization for both charge and discharge processes between the two types of electrodes are clearly observed. Moreover, the increase in overpotential became more evident for the uncoated electrode as the cycling progressed, compared to the coated electrode. Further evidence for this is the voltage gap between the charge and discharge profiles at 60 mAh/g in **Figure 2b and 2d**. These are plotted in **Figure 2e**. It is clear that there is a much larger gap for the cells containing the uncoated samples compared to those with the coated ones and that the polarization rises more rapidly with cycle number. The rise in overpotential caused an apparent capacity decay when the cell was cycled, due to the limited voltage window, and suggests that there was a rise in impedance. To verify this, EIS were measured before cycling (shown in Figure S2) and after set numbers of cycles at C/5 at 4.7V for cells in the charged state; see Figure 2f. The plots in the figure correspond to 1^{st} cycle, 10^{th} cycle, 25^{th} cycle and 35^{th} cycle, respectively. An increase in charge transfer resistance during cycling can be clearly seen but the increase in uncoated sample is obviously larger than the coated one. Compared to the data for

the cell with the coated sample, the larger semicircle radius seen in the high frequency part of the Nyquist plot of the cell with the uncoated sample suggests that there is higher charge transfer resistance for the latter. The results here are also consistent with our previous EIS study on the cells cycled at C/2. The charge transfer resistance is related to surface properties of the electrodes and an increase is associated with deterioration of battery performance. The impedance and overpotential data demonstrate that an ultrathin surface modification with Al_2O_3 can effectively suppress the increase in impedance of the batteries, and hence improve the battery performance. To obtain further insights related to the above phenomena, the surface properties of the electrodes were examined, as described below.

2.3 Post-cycling characterization

Because of the low penetration depth of soft X-rays, XAS can be an excellent tool for studying surface phenomena. The transition metal L-edge XAS measures the electric dipole allowed electron transition from 2p to unfilled 3d orbitals. In this case, L-edge X-ray absorption spectra are ideal for studying the transition metal 3d states to examine their redox states. The L-edge spectra of Ni and Mn for both coated and uncoated samples after 35 cycles at C/5 are presented in **Figure 3a and 3b**. The spectra of the pristine samples are also provided for comparison.

From the Ni L-edge spectra in total electron yield (TEY) mode, which probes about 5 nm deep from the surface, there is clear evidence for the

oxidation of Ni from Ni^{2+} to Ni^{2+x} state after charging and reduction back to Ni^{2+} after discharging. The ratio of the intensities of the two peaks in the Ni L_3 region changed, with the higher frequency peak increasing upon oxidation and vice versa. This corresponds to the main reaction of $LiNi_{0.5}Mn_{1.5}O_4$, whose primary capacity comes from the Ni^{2+}/ Ni^{2+x} redox couple. The results may be complicated by possible surface reactions of the nickel; in nickel-containing layered oxides, surface Ni is often found to be in a lower oxidation state than that in the bulk at the top of charge. A comparison of the Ni L_3 peak ratios in the spectra of the coated and uncoated $LiNi_{0.5}Mn_{1.5}O_4$ electrodes in the charged state shows a slightly higher Ni oxidation state in the former compared to the latter, judging from the peak at 854 eV(pointed out with arrows in Figure 3a). This suggests that the ALD coating provides some protection against the surface reconstruction phenomenon that leads to lower average oxidation states of transition metals on particle surfaces.

More interesting results are revealed in the spectra for the Mn L-edges. There is little difference between the coated and uncoated samples in the charged states. The spectra of the charged electrodes also look very similar to that of the electrodes in the pristine state, consistent with the fact that most of the Mn in $LiNi_{0.5}Mn_{1.5}O_4$ is not electroactive. However, the Mn L-edge spectra obtained on electrodes in the discharged state show distinct differences between the coated and uncoated samples, with far less Mn^{2+} appearing in the former, judging from the relative intensities at 640 eV(pointed out with arrows in Figure 3b). As a reference for

Mn^{2+}octahedrally coordinated to oxygen, the Mn L-edge spectrum for $LiMnPO_4$ is also shown. The results indicate that Mn^{2+} is formed during the discharge process and is re-oxidized during charge. With the ALD coating, the Mn^{2+} evolution is effectively suppressed. This is also consistent with the differences in coulombic efficiencies observed between the coated and uncoated samples, where the ALD coated samples showed slightly higher coulombic efficiency than the uncoated ones (~98.8% *vs*. ~98.2%, **Figure S1**).

In the literature, different $LiNi_{0.5}Mn_{1.5}O_4$/electrolyte interface reactions have been reported by different groups with various measurements, including XPS, XAS, neutron reflectometry, optical fluorescence spectroscopy and so on. Several Mn-related products were discovered and reported, such as MnF_2, Mn^{2+} oxalates and carbonates, and Mn^{2+}/$^{3+}$ complexes with β-diketonate ligands, although the exact reaction process is still unclear and under investigation. Qiao *et al.* have reported that Mn dissolution in $LiNi_{0.5}Mn_{1.5}O_4$ is correlated with electrolyte/electrode interactions rather than Mn^{3+} disproportion. Jarry *et al.* also reported the formation of Mn containing species *via* reactions between the electrolyte and surfaces of $LiNi_{0.5}Mn_{1.5}O_4$ particles. The results here support the analysis that the main reason for the Mn^{2+} evolution is the reaction with electrolyte, rather than Mn^{3+} disproportion, as the Mn^{3+} plateau did not change much in the charge-discharge curves of the uncoated samples whereas the Mn^{2+} evolution is obvious. In the coated electrodes, all the surfaces exposed to electrolyte are covered with Al_2O_3, since it is known that the ALD

precursors can diffuse through the pores in the electrodes and conformally coat them. This inhibits direct contact between $LiNi_{0.5}Mn_{1.5}O_4$ and electrolyte suppressing the side reactions that form Mn^{2+}. As a result, the coated samples show much less Mn^{2+} evolution than the uncoated ones. In full cells with graphite anodes, Mn was found to deposit onto the anode causing deterioration of the performance, especially capacity decay and impedance buildup,. Also, the Mn reduction and deposition on the anode leads to reduced coulomb efficiency. Thus, adding a conformal coating layer *via* ALD can be an effective strategy to enhance battery performance.

Besides Mn^{2+} formation and dissolution, it has also been reported that the transition metal ions in the surface region can migrate into the tetrahedral Li sites and empty octahedral sites upon cycling, resulting in the formation of Mn_3O_4-like and rock-salt structures on the surface, accompanied by loss of surface oxygen. Mn^{2+} occupancy of the tetrahedral Li sites would lead to a Mn_3O_4-like spinel structure in $LiNi_{0.5}Mn_{1.5}O_4$. The formation of the Mn_3O_4-like and rock-salt structures on the surface is also related to the densification of the atomic structure and the buildup of charge transfer resistance.

As surface reconstruction is intrinsic to $LiNi_{0.5}Mn_{1.5}O_4$, as evidenced in literature, it will not be prevented by surface modifications such as coating, but surface modification can slow down the surface reconstruction. Since surface Mn_3O_4 is highly correlated to Mn^{2+}

dissolution, we believe less Mn dissolution can induce less Mn migration in the lattice during cycling, which can lead to a protection against the evolution of further structural transformation and buildup of resistance. Further in-depth study will be needed to gain advanced knowledge on this phenomenon, and to guide future study surface modification strategies such as the fine tuning of coating thickness.

This also coincides with X-ray Photoelectron Spectroscopy (XPS) and Time-of-Flight Secondary Ion Mass Spectrometry (TOFSIMS) results in the recent literature showing that coatings can lead to thinner cathode-electrolyte interface layers. The obvious differences between the coated and uncoated electrodes seen in the XAS measurements implies that the increased impedance comes from surface reactions of the $LiNi_{0.5}Mn_{1.5}O_4$, and that the ultrathin layer of Al_2O_3 on electrode surfaces can effectively suppress this phenomenon to a large extent. We note here that there should be an optimized thickness of the coating layer especially when the coating material is an insulator such as Al_2O_3. Thicker coatings might be more effective for surface modification but may also increase the electron transfer resistance and have a negative effect on the power performance of the batteries. The ability to exert good control over the thicknesses of the conformal coatings, even down to the atomic level, however, makes ALD an ideal process for fabricating protected electrodes .

XAS results are ensemble-averaged and show signals from numerous particles in the electrodes. To obtain detailed information on individual

particles, STEM imaging was performed. We investigated the surface Mn oxidation states of $LiNi_{0.5}Mn_{1.5}O_4$ particles in the discharged state after cycling, using STEM-EELS. The EELS line scan profiles are shown in the STEM images for particles from both coated and uncoated samples in the right side of **Figure 4a and 4b**, with the first 9 spectra from the very surface presented on the left side. The step sizes for the EELS scans are 1.5 nm. The scan direction is from surface to bulk, as indicated by the purple arrows in the figures. Note that while the ALD coating did not cover every surface of every particle, it was possible to obtain consistent results from several particles selected from the coated sample.

The onset energy shifted to higher energy in both coated and uncoated samples, showing that there is some variation of Mn oxidation state from surface to bulk present in both samples. Pairs of individual spectra from the two different electrodes at the 2^{nd} to 10^{th} depth are also presented in **Figure S3a to S3i**, with four representative comparisons (2^{nd}, 3^{rd} first and last two spectra from the 10 spectra) also shown in **Figure 4c**. We note here the spectra from the 1^{st} step (in black in the figures) were omitted from the comparison, since the spectrum from the surface of uncoated sample did not show any signal from Mn, which may be due to CEI formation on the surface blocking the signal. The pairwise comparison shows that the differences between the two samples are more obvious at the surface and less noticeable when going into the bulk. This indicates the average oxidation state of Mn in the coated sample is higher than uncoated at the very surfaces of the particles. Upon scanning deeper from

the surface, the difference in the oxidation states of Mn became less pronounced.

The results from the EELS measurements imply that the function of coating on $LiNi_{0.5}Mn_{1.5}O_4$ is to suppress the surface reaction that causes Mn^{2+} to form, but it does not entirely eliminate this phenomenon. This is also in agreement with the electrochemical data where an increase of the overpotential and charge transfer resistance was still observed in the cells with the coated electrodes, albeit to a lesser degree than in the ones with uncoated electrodes.

3. Conclusion

We studied the mechanism of the effect of ultrathin surface coatings on spinel $LiNi_{0.5}Mn_{1.5}O_4$. Complementary measurements including nanoscale STEM-EELS on the surface at the particle level, ensemble-averaged synchrotron X-ray absorption spectroscopy (XAS) at the electrode level, and EIS and galvanostatic cycling at the cell level were combined in this study. The XAS results showed clear evidence that the ALD coating effectively suppresses the formation of Mn^{2+} on the surface of the electrodes, which occurs because of the reaction with electrolyte on surfaces of the $LiNi_{0.5}Mn_{1.5}O_4$ particles. The spatially resolved STEM-EELS showed that Mn^{2+} evolution occurs on the surfaces of both coated and uncoated $LiNi_{0.5}Mn_{1.5}O_4$ particles, but to a much lesser degree for the former. The ALD coating partially protects particle surfaces by avoiding direct contact of $LiNi_{0.5}Mn_{1.5}O_4$ and electrolyte, and decelerates the

impedance buildup, resulting in less apparent capacity fading. The electrochemical data acquired at the cell level is consistent with the XAS observations at the electrode level and the EELS results at the particle level. Our findings also suggest that an optimization of coating thickness as well as coating material and coating process should be carefully studied in order to maximize the improvement achieved by surface modification of the battery materials. The results reported here can provide guidance for the development of strategies to improve battery performance by surface modification of cathodes.

4. Experimental Section

Material synthesis

A solid-state reaction was used to synthesize $LiNi_{0.5}Mn_{1.5}O_4$ particles. Typically, nickel acetate ($Ni(Ac)_2 \bullet 4H_2O$) and manganese acetate ($Mn(Ac)_2 \bullet 4H_2O$) were mixed at a molar ratio of Ni : Mn = 1 : 3 and hand milled in a mortar. After heating at 500 ºC for 5 hours, lithium acetate ($LiAc \bullet 2H_2O$) was added to the mixture with a molar ratio of Li : Ni : Mn = 2.1 : 1 : 3 (5% excess Li source was added in order to make up for the volatilization of Li during calcination), and the mixture was heated to 500 ºC for 5 hours once more. We note here the amount of lithium acetate added in this step was critical. In addition, since the top portion of the mixture experienced more Li source volatilization, the total amount of precursors used in each round was fine-tuned to minimize the influence from Li source volatilization. The details can be found in the supporting information. After adding lithium acetate, the mixture was milled again

and sintered at 950 ºC for 10 hours followed by annealing at 700 ºC for 10 hours. The product was naturally cooled in air.

ALD process

ALD was performed on pre-fabricated electrodes using a home-made system. Pneumatic valves were used to control the pulse of the precursors and a tube furnace was used as reaction chamber. A programmable logic controller controlled the valves. Trimethylaluminum (TMA) and H_2O were used as precursors. 10 cycles of ALD were performed at the temperature of 90 ºC and pressure of $6x10^{-1}$ torr. Here one cycle of ALD refers to the deposition of H_2O and TMA each for one time. The electrodes were prepared using a traditional slurry casting method on Al current collectors. The weight ratio in the electrodes was active material : poly(vinylidene fluoride) : carbon black = 8 : 1 : 1. The active material loading was about 3.5 mg/cm^2. After the ALD process, the electrodes were used directly without further annealing.

Electrochemical measurements

CR 2032 coin cells were assembled with Li metal as counter electrodes. A 1.2 M solution of $LiPF_6$ in ethylene carbonate (EC) and dimethyl carbonate (DMC) (3:7) was used as the electrolytic solution. The batteries were cycled in the voltage range of 3.5 V ~ 5 V. After a constant current charge, the batteries were charged at constant voltage of 5 V for either 30 min or until the current decreased to less than 0.01 mA, whichever came first. 1C rate is defined as 140 mA/g for this work. Electrochemical impedance

spectra (EIS) were collected in a two-electrode configuration with AC voltage at 5 mV amplitude and a frequency range of 100 kHz to 10 mHz. The batteries were fully charged and then rested overnight to reach equilibrium before the impedance test.

XRD

XRD measurements were performed on a Rigaku Ultima IV X-ray diffractometer with Cu as X-ray tube target. The operating voltage is 40 kV and current is 44 mA. The scan rate was 4 degree/min.

Synchrotron XAS

Batteries were disassembled in an argon filled glovebox after 35 cycles in either the charged or discharged state, as noted in the text and figures. Electrodes were rinsed with DMC and dried in the glovebox before being sealed into airtight bottles and transferred for the XAS measurements. XAS measurements were performed on the 31-pole wiggler beamline 10-1 at Stanford Synchrotron Radiation Light Source using a ring current of 350 mA and a 1000 l/mm spherical grating monochromator with 20 µm entrance and exit slits, providing ~10^{11} ph/s at 0.2 eV resolution in a 1 mm^2 beam spot. All samples were attached to an aluminum holder using conductive carbon tape. Data were collected under high vacuum of 10^{-9} torr in a single load at room temperature. The sample drain current was collected for total electron yield (TEY). All spectra were normalized by the current from freshly evaporated gold on a fine grid positioned upstream of the main chamber.

STEM-EELS measurements

The electrodes were in the fully discharged state when the batteries were opened up in the glovebox and rinsed with DMC. The particles were scratched off the electrodes and washed with NMP to remove the PVDF binder. The samples were dried at 50 ºC under vacuum before taking the EELS measurements. STEM-EELS measurements were performed with a JEOL JEM-2100F TEM equipped with an electron energy loss spectrometer (GIF Quantum SE). The electron's accelerating voltage was 200 kV. The line scanning direction from surface to bulk had a step size of 1.5 nm.

Supporting Information
Supporting Information is available from the Wiley Online Library or from the author.

Acknowledgements
We would like to acknowledge the collaboration of this research with King Abdul-Aziz City for Science and Technology (KACST) *via* The Center of Excellence for Green Nanotechnologies (CEGN). The synchrotron X-ray portions of this research were carried out at the Stanford Synchrotron Radiation Lightsource, a Directorate of SLAC National Accelerator Laboratory and an Office of Science User Facility operated for the US Department of Energy Office of Science by Stanford University (No. DE-AC02-76SF00515). The STEM-EELS experiments were carried out at the Center for Electron Microscopy and Microanalysis at the University of Southern California. We acknowledge the help from Dr. Steve Cronin's group for EIS measurements. Portions of the work carried out at Lawrence Berkeley National Laboratory was supported by the Assistant Secretary for Energy Efficiency and Renewable Energy, Office of Vehicle Technologies of the U.S. Department of Energy (DOE) under Contract No. DE-AC02-05CH11231. F.L. gratefully acknowledges Virginia Tech Department of Chemistry startup funds.

Received: ((will be filled in by the editorial staff))
Revised: ((will be filled in by the editorial staff))
Published online: ((will be filled in by the editorial staff))

References

[1] M. Armand, J. M. Tarascon, Nature 2008, 451, 652; J. M. Tarascon, M. Armand, Nature 2001, 414, 359; J. B. Goodenough, K. S. Park, J Am Chem Soc 2013, 135, 1167.
[2] J. B. Goodenough, A. Manthiram, Mrs Commun 2014, 4, 135; J. B. Goodenough, Y. Kim, J Power Sources 2011, 196, 6688.
[3] J. B. Goodenough, Energ Environ Sci 2014, 7, 14.
[4] A. Ulvestad, A. Singer, J. N. Clark, H. M. Cho, J. W. Kim, R. Harder, J. Maser, Y. S. Meng, O. G. Shpyrko, Science 2015, 348, 1344; H. G. Jung, M. W. Jang, J. Hassoun, Y. K. Sun, B. Scrosati, Nat Commun 2011, 2.
[5] Y. K. Sun, S. T. Myung, B. C. Park, J. Prakash, I. Belharouak, K. Amine, Nat Mater 2009, 8, 320; Y. K. Sun, Z. H. Chen, H. J. Noh, D. J. Lee, H. G. Jung, Y. Ren, S. Wang, C. S. Yoon, S. T. Myung, K. Amine, Nat Mater 2012, 11, 942; H. Wu, G. Chan, J. W. Choi, I. Ryu, Y. Yao, M. T. McDowell, S. W. Lee, A. Jackson, Y. Yang, L. B. Hu, Y. Cui, Nat Nanotechnol 2012, 7, 309; N. Liu, Z. D. Lu, J. Zhao, M. T. McDowell, H. W. Lee, W. T. Zhao, Y. Cui, Nat Nanotechnol 2014, 9, 187; J. Liu, A. Manthiram, J Electrochem Soc 2009, 156, S13; G. Alva, C. Kim, T. H. Yi, J. B. Cook, L. P. Xu, G. M. Nolis, J. Cabana, J Phys Chem C 2014, 118, 10596; S. Kuppan, H. Duncan, G. Y. Chen, Phys Chem Chem Phys 2015, 17, 26471.
[6] J. Liu, A. Manthiram, Chem Mater 2009, 21, 1695.
[7] N. Liu, H. Wu, M. T. McDowell, Y. Yao, C. M. Wang, Y. Cui, Nano Lett 2012, 12, 3315; Z. W. Seh, W. Y. Li, J. J. Cha, G. Y. Zheng, Y. Yang, M. T. McDowell, P. C. Hsu, Y. Cui, Nat Commun 2013, 4; X. Xiao, J. Kim, Z. Liu, *US Patent*, 2013; X. Xiao, M. W. Verbrugge, J. Wang, S., P. Liu, *US Patent*, 2012; Y. S. Jung, A. S. Cavanagh, Y. F. Yan, S. M. George, A. Manthiram, J Electrochem Soc 2011, 158, A1298; I. D. Scott, Y. S. Jung, A. S. Cavanagh, Y. F. An, A. C. Dillon, S. M. George, S. H. Lee, Nano Lett 2011, 11, 414; Y. H. Liu, X. Fang, M. Y. Ge, J. P. Rong, C. F. Shen, A. Y. Zhang, H. A. Enaya, C. W. Zhou, Nano Energy 2015, 16, 399; Y. H. Liu, X. Fang, A. Y. Zhang, C. F. Shen, Q. Z. Liu, H. A. Enaya, C. W. Zhou, Nano Energy 2016, 27, 27.
[8] Y. S. Jung, A. S. Cavanagh, L. A. Riley, S. H. Kang, A. C. Dillon, M. D. Groner, S. M. George, S. H. Lee, Adv Mater 2010, 22, 2172.
[9] J. Arrebola, A. Caballero, L. Hernan, J. Morales, E. R. Castellon, J. R. R. Barrado, J Electrochem Soc 2007, 154, A178.
[10] J. Arrebola, A. Caballero, L. Hernan, J. Morales, E. R. Castellon, Electrochem Solid St 2005, 8, A303.
[11] H. B. Kang, S. T. Myung, K. Amine, S. M. Lee, Y. K. Sun, J Power Sources 2010, 195, 2023.
[12] R. Alcantara, M. Jaraba, P. Lavela, J. L. Tirado, J Electroanal Chem 2004, 566, 187.
[13] Y. K. Sun, Y. S. Lee, M. Yoshio, K. Amine, Electrochem Solid St 2002, 5, A99.
[14] H. M. Wu, I. Belharouak, A. Abouimrane, Y. K. Sun, K. Amine, J Power Sources 2010, 195, 2909.
[15] J. G. Li, Y. Y. Zhang, J. J. Li, L. Wang, X. M. He, J. Gao, Ionics 2011, 17, 671.
[16] T. Y. Yang, N. Q. Zhang, Y. Lang, K. N. Sun, Electrochim Acta 2011, 56, 4058.
[17] J. H. Cho, J. H. Park, M. H. Lee, H. K. Song, S. Y. Lee, Energ Environ Sci 2012, 5, 7124.
[18] X. Fang, M. Y. Ge, J. P. Rong, C. W. Zhou, J Mater Chem A 2013, 1, 4083.
[19] X. Fang, M. Y. Ge, J. P. Rong, Y. C. Che, N. Aroonyadet, X. L. Wang, Y. H. Liu, A. Y. Zhang, C. W. Zhou, Energy Technol-Ger 2014, 2, 159.
[20] H. M. Cho, M. V. Chen, A. C. MacRae, Y. S. Meng, Acs Appl Mater Inter 2015, 7, 16231; J. Song, X. G. Han, K. J. Gaskell, K. Xu, S. B. Lee, L. B. Hu, J Nanopart Res 2014, 16.
[21] X. Fang, Y. Lu, N. Ding, X. Y. Feng, C. Liu, C. H. Chen, Electrochim Acta 2010, 55, 832.
[22] J. H. Kim, S. T. Myung, C. S. Yoon, S. G. Kang, Y. K. Sun, Chem Mater 2004, 16, 906.
[23] S. M. George, Chem Rev 2010, 110, 111; X. B. Meng, X. Q. Yang, X. L. Sun, Adv Mater 2012, 24, 3589; R. L. Puurunen, J Appl Phys 2005, 97.
[24] Q. M. Zhong, A. Bonakdarpour, M. J. Zhang, Y. Gao, J. R. Dahn, J Electrochem Soc 1997, 144, 205.
[25] J. Xiao, X. L. Chen, P. V. Sushko, M. L. Sushko, L. Kovarik, J. J. Feng, Z. Q. Deng, J. M. Zheng, G. L. Graff, Z. M. Nie, D. W. Choi, J. Liu, J. G. Zhang, M. S. Whittingham, Adv Mater 2012, 24, 2109.

[26] J. Lu, C. Zhan, T. P. Wu, J. G. Wen, Y. Lei, A. J. Kropf, H. M. Wu, D. J. Miller, J. W. Elam, Y. K. Sun, X. P. Qiu, K. Amine, Nat Commun 2014, 5.
[27] E. Peled, D. Golodnitsky, G. Ardel, J Electrochem Soc 1997, 144, L208; M. D. Levi, D. Aurbach, J Phys Chem B 1997, 101, 4630.
[28] F. Lin, I. M. Markus, D. Nordlund, T. C. Weng, M. D. Asta, H. L. L. Xin, M. M. Doeff, Nat Commun 2014, 5; F. Lin, D. Nordlund, T. C. Weng, Y. Zhu, C. M. Ban, R. M. Richards, H. L. Xin, Nat Commun 2014, 5; X. S. Liu, D. D. Wang, G. Liu, V. Srinivasan, Z. Liu, Z. Hussain, W. L. Yang, Nat Commun 2013, 4.
[29] R. M. Qiao, Y. S. Wang, P. Olalde-Velasco, H. Li, Y. S. Hu, W. L. Yang, J Power Sources 2015, 273, 1120.
[30] W. S. Yoon, M. Balasubramanian, K. Y. Chung, X. Q. Yang, J. McBreen, C. P. Grey, D. A. Fischer, J Am Chem Soc 2005, 127, 17479.
[31] F. Lin, D. Nordlund, I. M. Markus, T. C. Weng, H. L. Xin, M. M. Doeff, Energ Environ Sci 2014, 7, 3077.
[32] J. Ma, P. Hu, G. L. Cui, L. Q. Chen, Chem Mater 2016, 28, 3578; J. F. Browning, L. Baggetto, K. L. Jungjohann, Y. Wang, W. E. Tenhaeff, J. K. Keum, D. L. Wood, G. M. Veith, Acs Appl Mater Inter 2014, 6, 18569.
[33] A. Jarry, S. Gottis, Y. S. Yu, J. Roque-Rosell, C. Kim, J. Cabana, J. Kerr, R. Kostecki, J Am Chem Soc 2015, 137, 3533.
[34] N. P. W. Pieczonka, Z. Y. Liu, P. Lu, K. L. Olson, J. Moote, B. R. Powell, J. H. Kim, J Phys Chem C 2013, 117, 15947.
[35] X. Fang, N. Ding, X. Y. Feng, Y. Lu, C. H. Chen, Electrochim Acta 2009, 54, 7471.
[36] M. X. Lin, L. B. Ben, Y. Sun, H. Wang, Z. Z. Yang, L. Gu, X. Q. Yu, X. Q. Yang, H. F. Zhao, R. Yu, M. Armand, X. J. Huang, Chem Mater 2015, 27, 292.
[37] E. Y. Hu, S. M. Bak, J. Liu, X. Q. Yu, Y. N. Zhou, S. N. Ehrlich, X. Q. Yang, K. W. Nam, Chem Mater 2014, 26, 1108.
[38] J. M. Zheng, M. Gu, J. Xiao, P. J. Zuo, C. M. Wang, J. G. Zhang, Nano Lett 2013, 13, 3824; A. Boulineau, L. Simonin, J. F. Colin, C. Bourbon, S. Patoux, Nano Lett 2013, 13, 3857.
[39] A. Singer, A. Ulvestad, H. M. Cho, J. W. Kim, J. Maser, R. Harder, Y. S. Meng, O. G. Shpyrko, Nano Lett 2014, 14, 5295.
[40] D. C. Tang, Y. Sun, Z. Z. Yang, L. B. Ben, L. Gu, X. J. Huang, Chem Mater 2014, 26, 3535.
[41] J. W. Kim, D. H. Kim, D. Y. Oh, H. Lee, J. H. Kim, J. H. Lee, Y. S. Jung, J Power Sources 2015, 274, 1254.

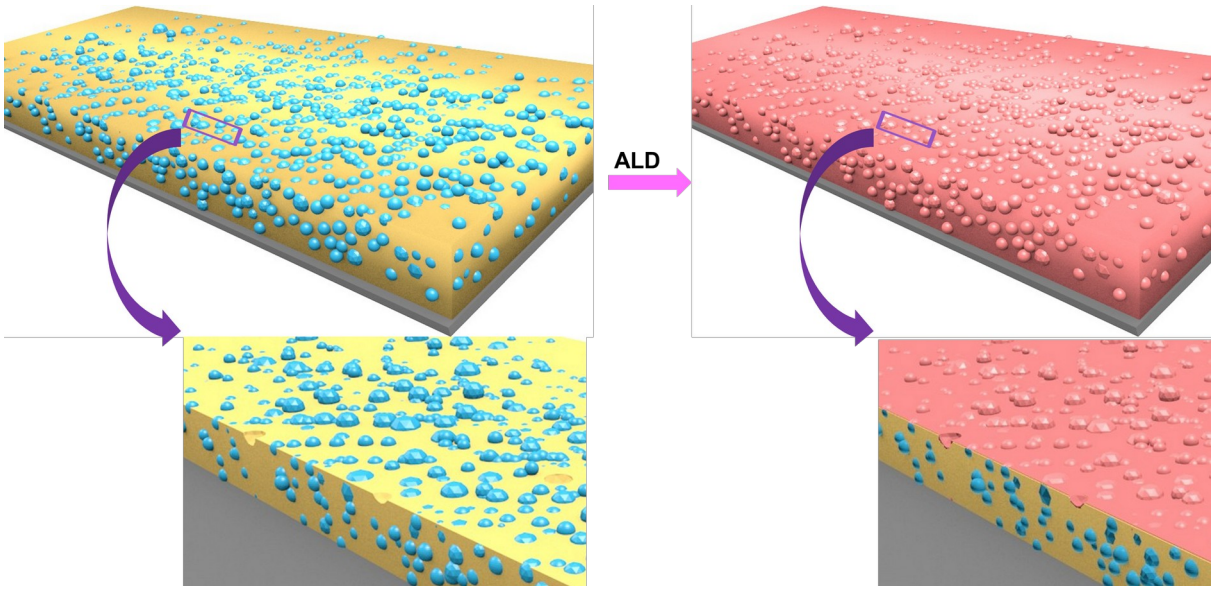

Scheme Schematic diagram showing ALD on pre-fabricated electrodes

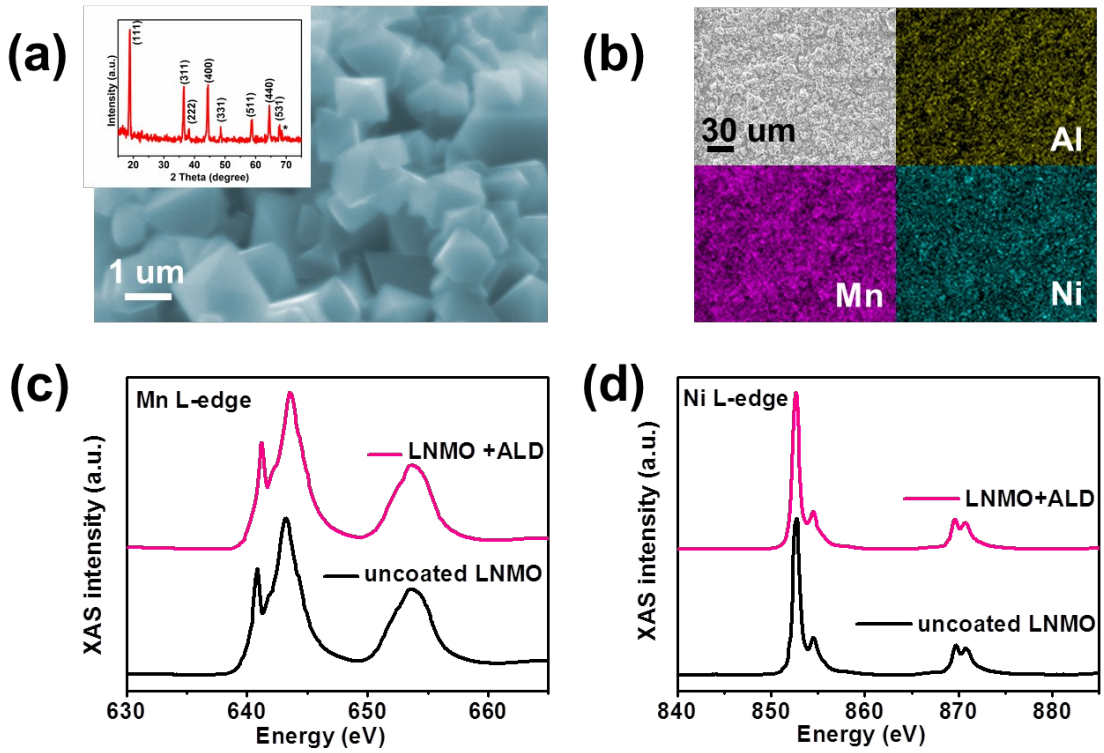

Figure 1. (a) SEM image and (inset) XRD pattern of the as-synthesized $LiNi_{0.5}Mn_{1.5}O_4$ particles before ALD coating. (b) EDX mapping of Al, Ni and Mn on the surface of the electrode after ALD coating. The mapping area is shown in the upper-left. XAS results of (c) Mn and (d) Ni of both coated and uncoated electrodes before cycling.

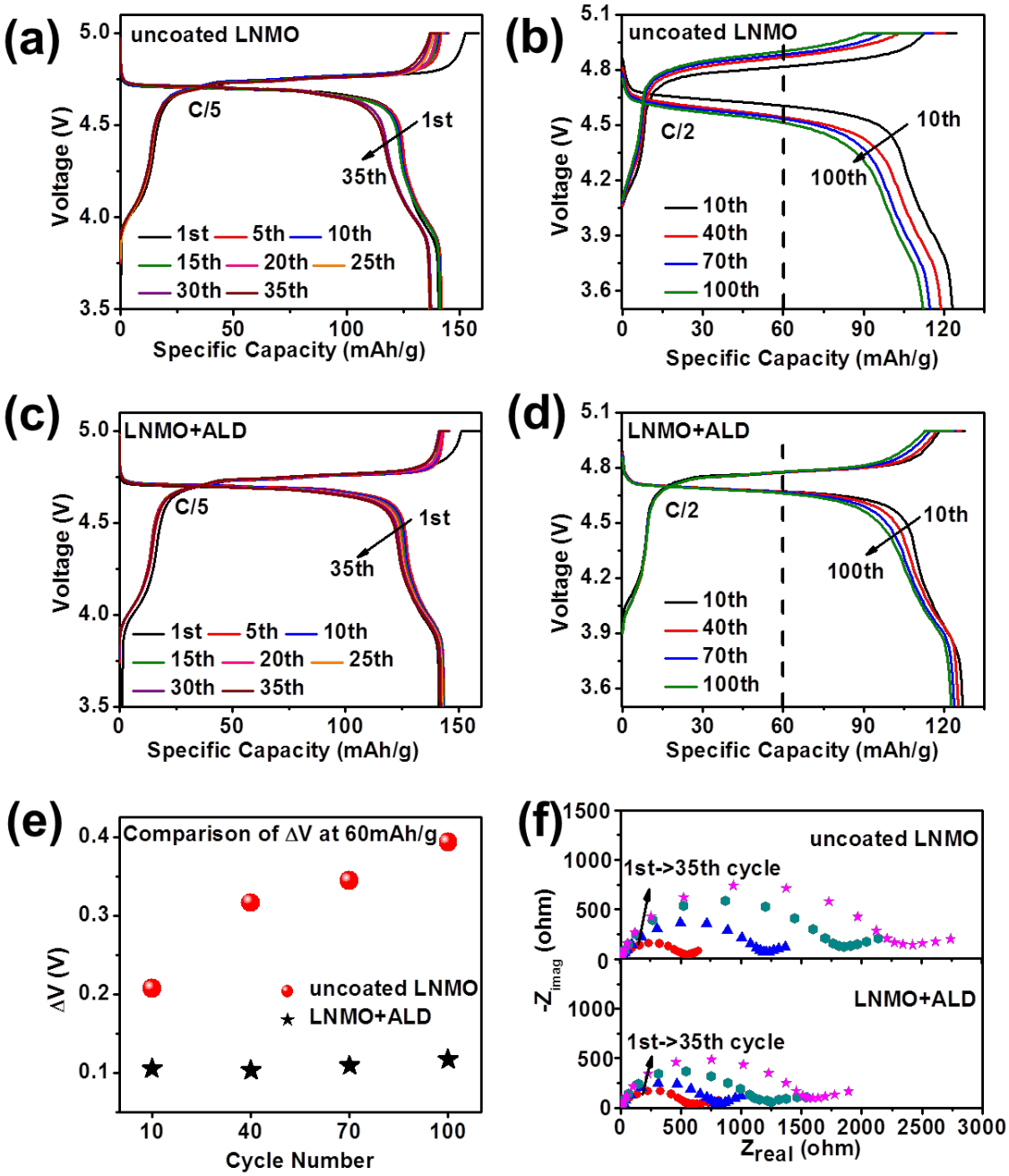

Figure 2. Representative charge-discharge curves of (a,b) uncoated and (c,d) coated $LiNi_{0.5}Mn_{1.5}O_4$ at C/5 and C/2 (1C = 140mA/g). (e) Comparison of voltage gap at 60 mAh/g of coated and uncoated electrodes at C/2. (f) Comparison of Nyquist plots for coated and uncoated electrodes in the charged state from 1st cycle, 10th cycle, 25th cycle and 35th cycle, respectively

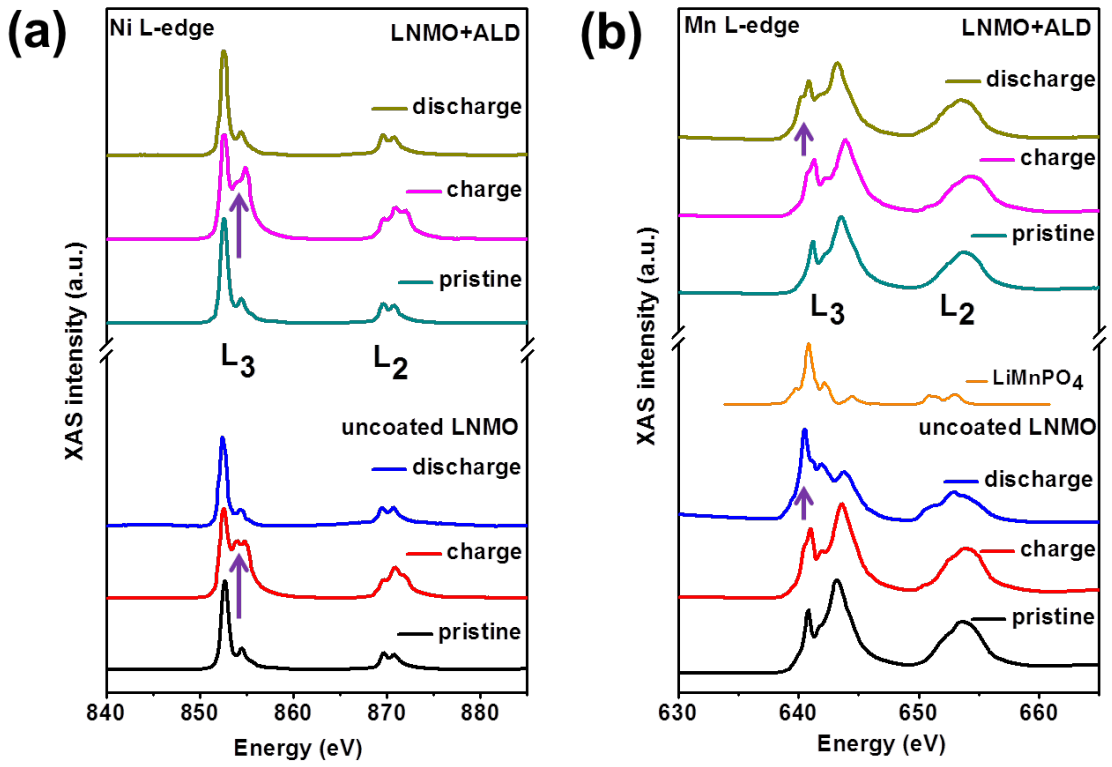

Figure 3. (a) Ni L-edge XAS/TEY spectra for uncoated and coated electrodes. (b) Mn L-edge XAS/TEY spectra for uncoated and coated electrodes. All spectra were collected from electrodes at the 35th cycle, in either the fully charged or fully discharged state, as noted in the figures. The electrodes in the charged state were taken out from batteries after constant voltage charge step and the ones at discharged state were taken from batteries after constant current discharge to 3.5 V.

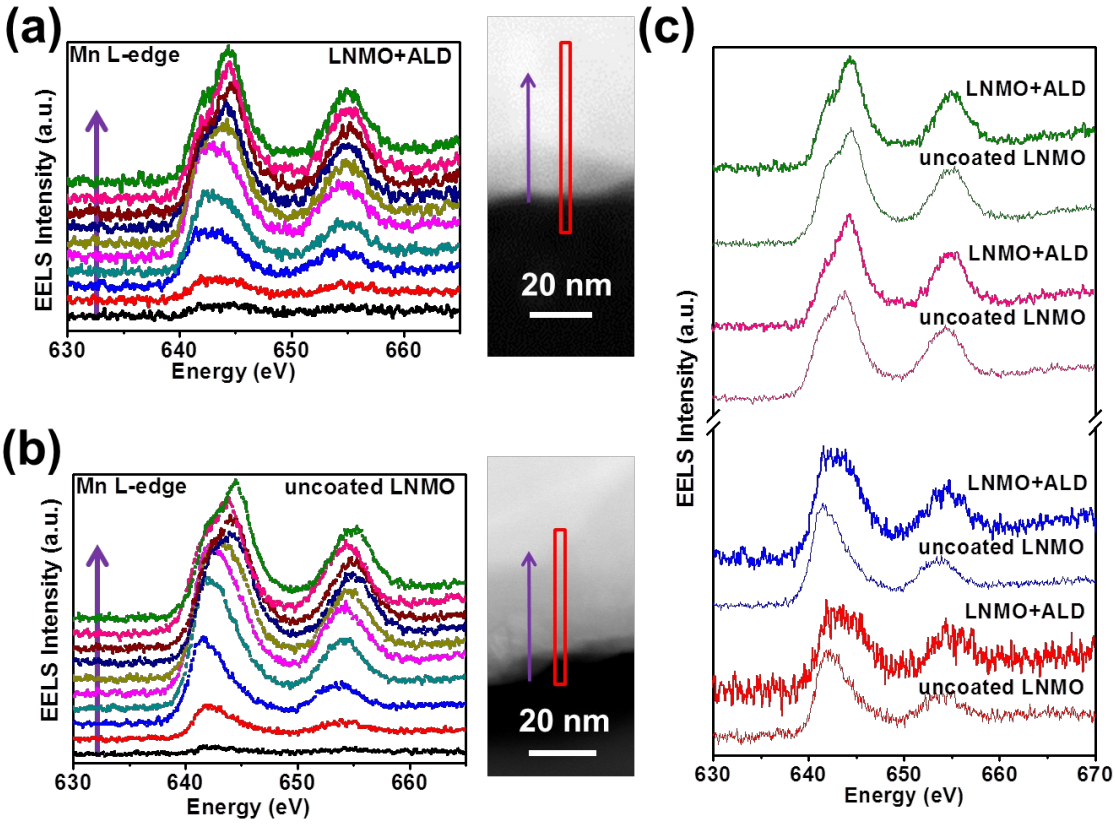

Figure 4. Mn L-edge spectra taken with EELS for particles from coated (a) and uncoated (b) electrodes after the 100th cycle. The STEM images showing the EELS scanning pathway were shown on the right side of the spectra. The step size in EELS scan was 1.5 nm and the first ten spectra from the surface of the particles were shown in (a) and (b). (c) Comparison of Mn L-edge spectra taken at the 2nd, 3rd, 9th and 10th steps shown in Figure 4a (denoted as LNMO+ALD), and Figure 4b (denoted as uncoated LNMO). The detailed comparisons of spectra taken at each depth were shown in Figure S3.

Atomic Layer Deposition is employed in ultrathin coating for high voltage cathode $LiNi_{0.5}Mn_{1.5}O_4$ in lithium ion batteries. Atomic insight into the enhanced stability of the uncoated electrodes is revealed by XAS and STEM-EELS study. The coating has been found to effectively suppress the Mn^{2+} evolution, and improves the battery performance by decelerating the impedance buildup from the surface passivation.

Keyword lithium ion batteries, high voltage cathode, $LiNi_{0.5}Mn_{1.5}O_4$, surface modification, Mn^{2+} evolution

Dr. X. Fang, Dr. M. Ge, Dr. J. Rong, A. Zhang, C. Shen, Prof. C. Zhou
Mork Family Department of Chemical Engineering and Materials Science, University of Southern California, Los Angeles, California 90089, United States
E-mail: chongwuz@usc.edu
Dr. F. Lin, Dr. M. M. Doeff
Energy Storage & Distributed Resources Division, Lawrence Berkeley National Laboratory, Berkeley, California 94720, USA
Dr. D. Nordlund
Stanford Synchrotron Radiation Lightsource, SLAC National Accelerator Laboratory, Menlo Park, California 94025, USA
Dr. M. Mecklenburg
Center for Electron Microscopy and Microanalysis, University of Southern California, Los Angeles, California 90089, USA
Y. Liu, Y. Cao, Prof. C. Zhou
Ming Hsieh Department of Electrical Engineering, University of Southern California, Los Angeles, California 90089, United States
Prof. F. Lin
Department of Chemistry, Virginia Tech, Blacksburg, VA 24061, USA

Atomic Insight into the Enhanced Surface Stability in High Voltage Cathode Materials by Ultrathin Coating

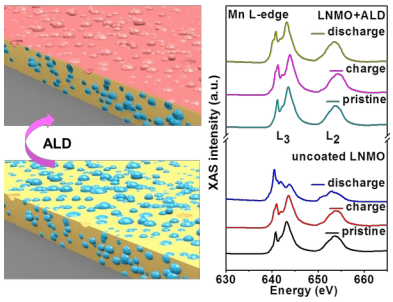

Supporting Information

Atomic Insights into the Enhanced Surface Stability in High Voltage Cathode Materials by Ultrathin Coating

Xin Fang,[†] Feng Lin[#§], Dennis Nordlund,[‖] Matthew Mecklenburg,[⊥] Mingyuan Ge,[†] Jiepeng Rong,[†] Anyi Zhang,[†] Chenfei Shen,[†] Yihang Liu,[‡] Yu Cao,[‡] Marca M. Doeff,[#] and Chongwu Zhou[†‡,]*

Dr. X. Fang, Dr. M. Ge, Dr. J. Rong, A. Zhang, C. Shen, Prof. C. Zhou
Mork Family Department of Chemical Engineering and Materials Science, University of Southern California, Los Angeles, California 90089, United States
E-mail: chongwuz@usc.edu
Dr. F. Lin, Dr. M. M. Doeff
Energy Storage & Distributed Resources Division, Lawrence Berkeley National Laboratory, Berkeley, California 94720, USA
Dr. D. Nordlund
Stanford Synchrotron Radiation Lightsource, SLAC National Accelerator Laboratory, Menlo Park, California 94025, USA
Dr. M. Mecklenburg
Center for Electron Microscopy and Microanalysis, University of Southern California, Los Angeles, California 90089, USA
Y. Liu, Y. Cao, Prof. C. Zhou
Ming Hsieh Department of Electrical Engineering, University of Southern California, Los Angeles, California 90089, United States
Prof. F. Lin
Department of Chemistry, Virginia Tech, Blacksburg, VA 24061, USA

Fine-tuning of $LiNi_{0.5}Mn_{1.5}O_4$ synthesis method

The amount of lithium acetate added in the second round of 500ºC heating will affect the quality of the final product. Since some of the nickel acetate and manganese acetate sticks to the wall of the crucible after heating, when adding Li source to the mixture, the amount is carefully calculated based on the actual amount of Ni and Mn sources taken out of the crucible, where anything stuck on the wall was excluded. In addition, since the top portion of the mixture experiences more Li source volatilization, the total amount of precursors used in each round was adjusted until the influence from Li source volatilization was minimized.

Figure S1

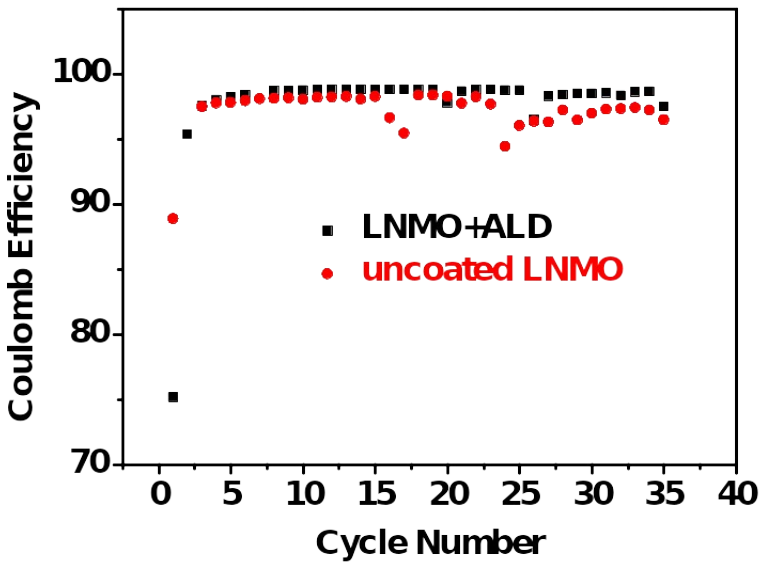

Figure S1. Coulombic efficiency of coated and uncoated samples cycled at C/5.

We note here we have tested more than 10 cells and the ones shown here are the ones used for XAS measurement. The mean values of first cycle coulombic efficiency between coated and uncoated samples are similar, 86.80% (coated) *vs.* 86.05% (uncoated). The slight difference may be due to the side reaction between electrolyte and $LiNi_{0.5}Mn_{1.5}O_4$,where in the uncoated samples the reaction is more severe and leads to a slightly lower first cycle coulombic efficiency.

EIS measured before cycling

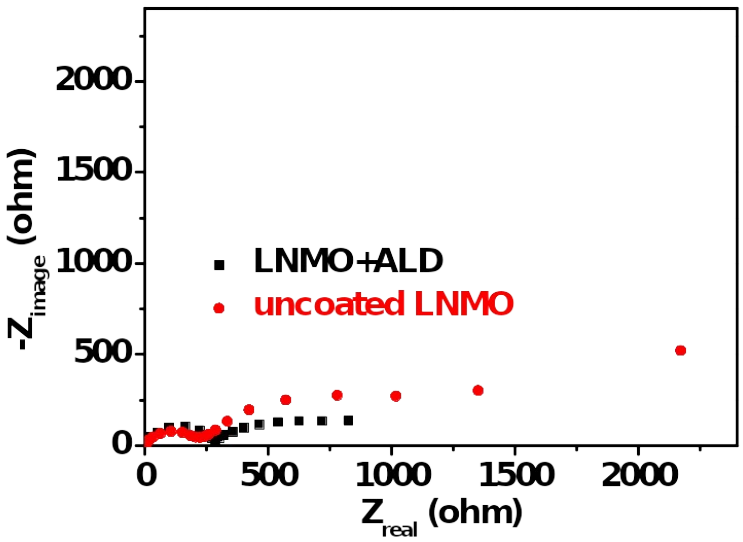

Figure S2 Comparison of EIS before cycling

EIS data on cells measured before cycling is shown in Figure S2. The cell containing the ALD coated sample showed a slightly larger charge transfer resistance which might be caused by the added Al_2O_3 layer.

EELS profiles at each depth of scanning

Figure S3

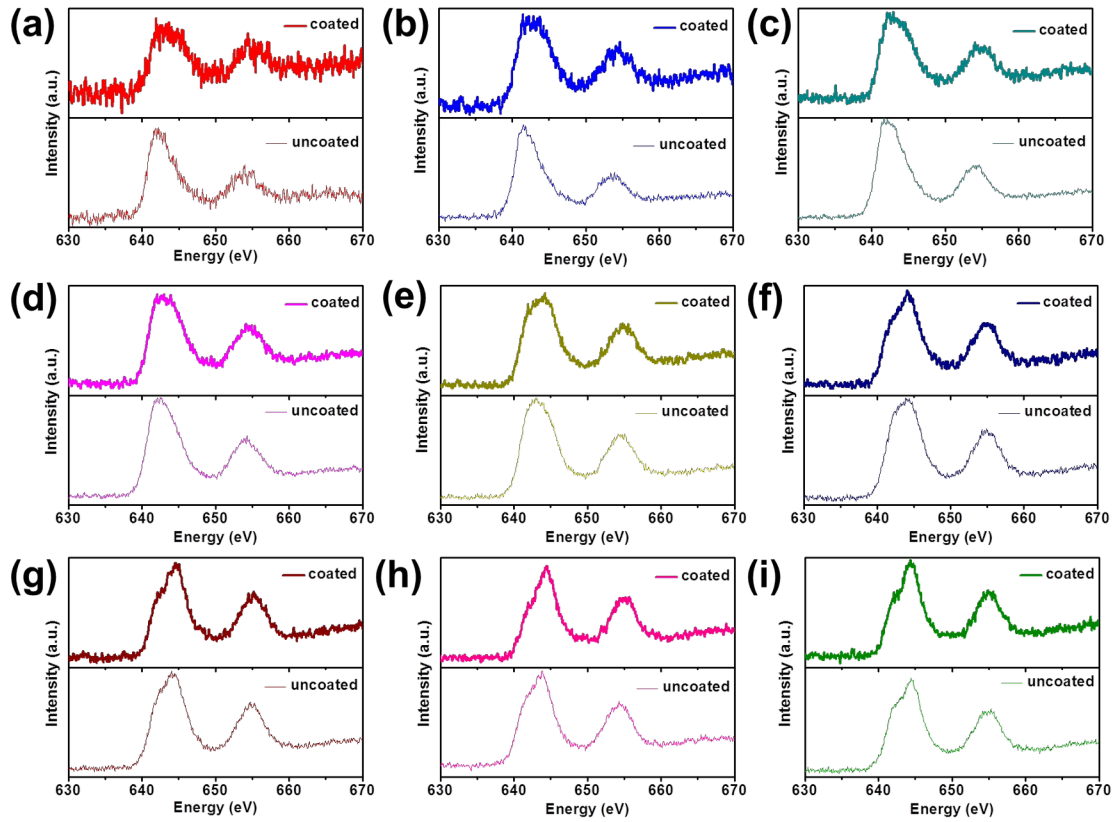

Figure S3. Comparison of EELS profiles for coated and uncoated samples shown in Figure 4a and 4b at each depth from surface (a) along the scanning path to bulk (i). Each color corresponds to the respective color in Figure 4a and 4b. Step size is 1.5 nm.

[1] M. Armand, J. M. Tarascon, Nature 2008, 451, 652; J. M. Tarascon, M. Armand, Nature 2001, 414, 359; J. B. Goodenough, K. S. Park, J Am Chem Soc 2013, 135, 1167.
[2] J. B. Goodenough, A. Manthiram, Mrs Commun 2014, 4, 135; J. B. Goodenough, Y. Kim, J Power Sources 2011, 196, 6688.
[3] J. B. Goodenough, Energ Environ Sci 2014, 7, 14.
[4] A. Ulvestad, A. Singer, J. N. Clark, H. M. Cho, J. W. Kim, R. Harder, J. Maser, Y. S. Meng, O. G. Shpyrko, Science 2015, 348, 1344; H. G. Jung, M. W. Jang, J. Hassoun, Y. K. Sun, B. Scrosati, Nat Commun 2011, 2.
[5] Y. K. Sun, S. T. Myung, B. C. Park, J. Prakash, I. Belharouak, K. Amine, Nat Mater 2009, 8, 320; Y. K. Sun, Z. H. Chen, H. J. Noh, D. J. Lee, H. G. Jung, Y. Ren, S. Wang, C. S. Yoon, S. T. Myung, K. Amine, Nat Mater 2012, 11, 942; H. Wu, G. Chan, J. W. Choi, I. Ryu, Y. Yao, M. T. McDowell, S. W. Lee, A. Jackson, Y. Yang, L. B. Hu, Y. Cui, Nat Nanotechnol 2012, 7, 309; N. Liu, Z. D. Lu, J. Zhao, M. T. McDowell, H. W. Lee, W. T. Zhao, Y. Cui, Nat

Nanotechnol 2014, 9, 187; J. Liu, A. Manthiram, J Electrochem Soc 2009, 156, S13; G. Alva, C. Kim, T. H. Yi, J. B. Cook, L. P. Xu, G. M. Nolis, J. Cabana, J Phys Chem C 2014, 118, 10596; S. Kuppan, H. Duncan, G. Y. Chen, Phys Chem Chem Phys 2015, 17, 26471.
[6] J. Liu, A. Manthiram, Chem Mater 2009, 21, 1695.
[7] N. Liu, H. Wu, M. T. McDowell, Y. Yao, C. M. Wang, Y. Cui, Nano Lett 2012, 12, 3315; Z. W. Seh, W. Y. Li, J. J. Cha, G. Y. Zheng, Y. Yang, M. T. McDowell, P. C. Hsu, Y. Cui, Nat Commun 2013, 4; X. Xiao, J. Kim, Z. Liu, *US Patent*, 2013; X. Xiao, M. W. Verbrugge, J. Wang, S., P. Liu, *US Patent*, 2012; Y. S. Jung, A. S. Cavanagh, Y. F. Yan, S. M. George, A. Manthiram, J Electrochem Soc 2011, 158, A1298; I. D. Scott, Y. S. Jung, A. S. Cavanagh, Y. F. An, A. C. Dillon, S. M. George, S. H. Lee, Nano Lett 2011, 11, 414; Y. H. Liu, X. Fang, M. Y. Ge, J. P. Rong, C. F. Shen, A. Y. Zhang, H. A. Enaya, C. W. Zhou, Nano Energy 2015, 16, 399; Y. H. Liu, X. Fang, A. Y. Zhang, C. F. Shen, Q. Z. Liu, H. A. Enaya, C. W. Zhou, Nano Energy 2016, 27, 27.
[8] Y. S. Jung, A. S. Cavanagh, L. A. Riley, S. H. Kang, A. C. Dillon, M. D. Groner, S. M. George, S. H. Lee, Adv Mater 2010, 22, 2172.
[9] J. Arrebola, A. Caballero, L. Hernan, J. Morales, E. R. Castellon, J. R. R. Barrado, J Electrochem Soc 2007, 154, A178.
[10] J. Arrebola, A. Caballero, L. Hernan, J. Morales, E. R. Castellon, Electrochem Solid St 2005, 8, A303.
[11] H. B. Kang, S. T. Myung, K. Amine, S. M. Lee, Y. K. Sun, J Power Sources 2010, 195, 2023.
[12] R. Alcantara, M. Jaraba, P. Lavela, J. L. Tirado, J Electroanal Chem 2004, 566, 187.
[13] Y. K. Sun, Y. S. Lee, M. Yoshio, K. Amine, Electrochem Solid St 2002, 5, A99.
[14] H. M. Wu, I. Belharouak, A. Abouimrane, Y. K. Sun, K. Amine, J Power Sources 2010, 195, 2909.
[15] J. G. Li, Y. Y. Zhang, J. J. Li, L. Wang, X. M. He, J. Gao, Ionics 2011, 17, 671.
[16] T. Y. Yang, N. Q. Zhang, Y. Lang, K. N. Sun, Electrochim Acta 2011, 56, 4058.
[17] J. H. Cho, J. H. Park, M. H. Lee, H. K. Song, S. Y. Lee, Energ Environ Sci 2012, 5, 7124.
[18] X. Fang, M. Y. Ge, J. P. Rong, C. W. Zhou, J Mater Chem A 2013, 1, 4083.
[19] X. Fang, M. Y. Ge, J. P. Rong, Y. C. Che, N. Aroonyadet, X. L. Wang, Y. H. Liu, A. Y. Zhang, C. W. Zhou, Energy Technol-Ger 2014, 2, 159.
[20] H. M. Cho, M. V. Chen, A. C. MacRae, Y. S. Meng, Acs Appl Mater Inter 2015, 7, 16231; J. Song, X. G. Han, K. J. Gaskell, K. Xu, S. B. Lee, L. B. Hu, J Nanopart Res 2014, 16.
[21] X. Fang, Y. Lu, N. Ding, X. Y. Feng, C. Liu, C. H. Chen, Electrochim Acta 2010, 55, 832.
[22] J. H. Kim, S. T. Myung, C. S. Yoon, S. G. Kang, Y. K. Sun, Chem Mater 2004, 16, 906.
[23] S. M. George, Chem Rev 2010, 110, 111; X. B. Meng, X. Q. Yang, X. L. Sun, Adv Mater 2012, 24, 3589; R. L. Puurunen, J Appl Phys 2005, 97.
[24] Q. M. Zhong, A. Bonakdarpour, M. J. Zhang, Y. Gao, J. R. Dahn, J Electrochem Soc 1997, 144, 205.

[25] J. Xiao, X. L. Chen, P. V. Sushko, M. L. Sushko, L. Kovarik, J. J. Feng, Z. Q. Deng, J. M. Zheng, G. L. Graff, Z. M. Nie, D. W. Choi, J. Liu, J. G. Zhang, M. S. Whittingham, Adv Mater 2012, 24, 2109.
[26] J. Lu, C. Zhan, T. P. Wu, J. G. Wen, Y. Lei, A. J. Kropf, H. M. Wu, D. J. Miller, J. W. Elam, Y. K. Sun, X. P. Qiu, K. Amine, Nat Commun 2014, 5.
[27] E. Peled, D. Golodnitsky, G. Ardel, J Electrochem Soc 1997, 144, L208; M. D. Levi, D. Aurbach, J Phys Chem B 1997, 101, 4630.
[28] F. Lin, I. M. Markus, D. Nordlund, T. C. Weng, M. D. Asta, H. L. L. Xin, M. M. Doeff, Nat Commun 2014, 5; F. Lin, D. Nordlund, T. C. Weng, Y. Zhu, C. M. Ban, R. M. Richards, H. L. Xin, Nat Commun 2014, 5; X. S. Liu, D. D. Wang, G. Liu, V. Srinivasan, Z. Liu, Z. Hussain, W. L. Yang, Nat Commun 2013, 4.
[29] R. M. Qiao, Y. S. Wang, P. Olalde-Velasco, H. Li, Y. S. Hu, W. L. Yang, J Power Sources 2015, 273, 1120.
[30] W. S. Yoon, M. Balasubramanian, K. Y. Chung, X. Q. Yang, J. McBreen, C. P. Grey, D. A. Fischer, J Am Chem Soc 2005, 127, 17479.
[31] F. Lin, D. Nordlund, I. M. Markus, T. C. Weng, H. L. Xin, M. M. Doeff, Energ Environ Sci 2014, 7, 3077.
[32] J. Ma, P. Hu, G. L. Cui, L. Q. Chen, Chem Mater 2016, 28, 3578; J. F. Browning, L. Baggetto, K. L. Jungjohann, Y. Wang, W. E. Tenhaeff, J. K. Keum, D. L. Wood, G. M. Veith, Acs Appl Mater Inter 2014, 6, 18569.
[33] A. Jarry, S. Gottis, Y. S. Yu, J. Roque-Rosell, C. Kim, J. Cabana, J. Kerr, R. Kostecki, J Am Chem Soc 2015, 137, 3533.
[34] N. P. W. Pieczonka, Z. Y. Liu, P. Lu, K. L. Olson, J. Moote, B. R. Powell, J. H. Kim, J Phys Chem C 2013, 117, 15947.
[35] X. Fang, N. Ding, X. Y. Feng, Y. Lu, C. H. Chen, Electrochim Acta 2009, 54, 7471.
[36] M. X. Lin, L. B. Ben, Y. Sun, H. Wang, Z. Z. Yang, L. Gu, X. Q. Yu, X. Q. Yang, H. F. Zhao, R. Yu, M. Armand, X. J. Huang, Chem Mater 2015, 27, 292.
[37] E. Y. Hu, S. M. Bak, J. Liu, X. Q. Yu, Y. N. Zhou, S. N. Ehrlich, X. Q. Yang, K. W. Nam, Chem Mater 2014, 26, 1108.
[38] J. M. Zheng, M. Gu, J. Xiao, P. J. Zuo, C. M. Wang, J. G. Zhang, Nano Lett 2013, 13, 3824; A. Boulineau, L. Simonin, J. F. Colin, C. Bourbon, S. Patoux, Nano Lett 2013, 13, 3857.
[39] A. Singer, A. Ulvestad, H. M. Cho, J. W. Kim, J. Maser, R. Harder, Y. S. Meng, O. G. Shpyrko, Nano Lett 2014, 14, 5295.
[40] D. C. Tang, Y. Sun, Z. Z. Yang, L. B. Ben, L. Gu, X. J. Huang, Chem Mater 2014, 26, 3535.
[41] J. W. Kim, D. H. Kim, D. Y. Oh, H. Lee, J. H. Kim, J. H. Lee, Y. S. Jung, J Power Sources 2015, 274, 1254.